Improved Airborne Hot-Wire Measurements of Ice Water Content in Clouds

ARTICLE *in* JOURNAL OF ATMOSPHERIC AND OCEANIC TECHNOLOGY · SEPTEMBER 2013

Impact Factor: 1.73 · DOI: 10.1175/JTECH-D-13-00007.1

4 AUTHORS, INCLUDING:

A. V. Korolev
Environment Canada
124 PUBLICATIONS **2,777** CITATIONS

Improved Airborne Hot-Wire Measurements of Ice Water Content in Clouds

A. KOROLEV, J. W. STRAPP, AND G. A. ISAAC

Cloud Physics and Severe Weather Research Section, Environment Canada, Toronto, Ontario, Canada

E. EMERY

NASA Glenn Research Center, Cleveland, Ohio

(Manuscript received 10 January 2013, in final form 18 March 2013)

ABSTRACT

Airborne measurements of ice water content (IWC) in both ice and mixed-phase clouds remain one of the long-standing problems in experimental cloud physics. For nearly three decades, IWC has been measured with the help of the Nevzorov hot-wire total water content (TWC) sensor, which had an inverted cone shape. It was assumed that ice particles would be captured inside the cone and then completely melt and evaporate. However, wind tunnel experiments conducted with the help of high-speed video recordings showed that ice particles may bounce out of the TWC cone, resulting in the underestimation of the measured IWC. The TWC sensor was modified to improve the capture efficiency of ice particles. The modified sensor was mounted on the National Research Council (NRC) Convair-580 and its measurements in ice clouds were compared with the measurements of the original Nevzorov TWC sensor, a Droplet Measurement Technologies (DMT) counterflow virtual impactor (CVI), and IWC calculated from the particle size distribution measured by optical array probes (OAPs). Results indicated that the IWC measured by the modified TWC hot-wire sensor as well as the CVI and that deduced from the OAP size distributions agreed reasonably well when the maximum size of ice particles did not exceed 4 mm. However, IWC measured by the original TWC sensor was approximately 3 times lower than that measured by the other three techniques. This result can be used for the retrieval of the past IWC measurements obtained with this TWC sensor. For clouds with ice particles larger than 4 mm, the IWC measured by the modified TWC sensor and CVI exhibited diverging measurements.

1. Introduction

Cloud water in solid state may be considered as one of the significant substances in the atmosphere affecting the water cycle and radiation budget of the earth. Measurements of the ice water content (IWC) is one of the fundamental requirements of applied cloud microphysics for validating weather predictions and climate models, remote sensing, and for developing safety standards for mobile platforms such airplanes, helicopters, balloons, etc.

Currently, there are three classes of techniques used in the measurement of IWC. The first technique involves the calculation of IWC from the measurements of particle size distribution, based on the size-to-mass conversion (e.g., Locatelli and Hobbs 1974; Brown and Francis 1995; Baker and Lawson 2006; Heymsfield et al. 2010; and others). The second technique consists of estimating IWC from the increase in water vapor density resulting from total evaporation of ice particles (e.g., Ruskin 1967; Kyle 1975; Ruskin 1976; Nicholls et al. 1990; Brown 1993; Twohy et al. 1997; Weinstock et al. 2006; Davis et al. 2007; Davison et al. 2009). The third technique utilizes the hot-wire technique (e.g., King and Turvey 1986; Nevzorov 1980, 1983; Korolev et al. 1998), where IWC is calculated from the measurements of power used for melting and evaporation of ice particles impacting the surface of a heated hot-wire sensor.

Despite the substantial efforts invested in the development of each of the above-mentioned techniques, there are still considerable uncertainties in the accuracy of IWC measurements. The existing problems result from multiple causes: 1) the large range of ice particle sizes covering four orders of magnitude, creating specific problems for in situ sampling and requirements for geometrical characteristics of the probes' inlets; 2) the

Corresponding author address: Alexei Korolev, Environment Canada, 4905 Dufferin Street, Toronto ON M3H5T4, Canada.
E-mail: alexei.korolev@ec.gc.ca

DOI: 10.1175/JTECH-D-13-00007.1

highly variable density of ice particles, which does not allow for unique coefficients for size-to-area parameterizations when deriving IWC from particle spectra, as opposed to the case of liquid droplets; and 3) the present lack of mature calibration standards for ice clouds in wind tunnels. Although some ice cloud simulations in wind tunnels show promise for absolute IWC calibration (e.g., Strapp et al. 2008), efforts are still ongoing in characterizing the reference IWC measurements in such tunnels. Since ice is produced artificially, there is also some debate as to how representative these conditions are of widely varying natural clouds. As a result, the most frequently used and commonly accepted assessment strategy is still through comparisons of multiple measurements by instruments utilizing different IWC techniques. Although this approach will not necessarily provide a direct answer about the absolute accuracy of the IWC measurements, it does provide better understanding of uncertainties in datasets being collected with different instruments, and it may reveal some specific measurement problems and help formulate new directions for future improvement of IWC instrumentation.

In the present paper, three IWC probe measurement techniques are compared: 1) the Sky Tech Research hot-wire Nevzorov probe (Korolev et al. 1998) with a modified total water content (TWC) sensor; 2) the counterflow virtual impactor (CVI; Twohy et al. 1997) component of the Droplet Measurement Technologies (DMT) cloud spectrometer and impactor (CSI), using the evaporation technique; and 3) Particle Measuring Systems (PMS) optical array probes (OAPs) OAP-2DC and OAP-2DP (Knollenberg 1981) with particle size distributions converted to IWC based on size-to-mass parameterization. The first part of the paper is focused on the problems inherent in the sampling of ice particles by the hot-wire sensors. The second part describes the intercomparisons of the IWC measured in situ by the Nevzorov probe, DMT CVI, and that deduced from particle size distributions.

2. High-speed video tests

The concept behind the IWC measurements made by the hot-wire Nevzorov TWC sensor is based on the assumption that ice particles remain inside the conical capture volume and then melt and evaporate (see Fig. 2b in Korolev et al. 1998). However, high-speed video of the of the interaction of the ice particles with the heated sensor surface reported by Emery et al. (2004) and Strapp et al. (2005) showed that some ice particles may bounce out of the Nevzorov TWC cone sensor and other hot-wire sensor geometries. The tests were conducted in the Cox & Co. LeClerc wind tunnel, which has the capability of producing an ice cloud by shaving ice blocks. The shaved ice particles have an irregular shape with a characteristic size ranging from 100 to 400 μm. The high-speed video was taken in the Cox & Co. wind tunnel with help of the Phantom v5.0 (v5) high-framerate camera manufactured by Vision Research, Inc. The pixel resolution of the camera was determined by the optical zoom settings, and for the experiments described below it ranged from approximately 50 to 100 μm.

Figure 1 shows images of the side view of the Nevzorov TWC sensor exposed to a flow of ice particles. As seen in Fig. 1, some of the particles rebound off the TWC cone into the airstream and are swept away, which results in an underestimate of the measured IWC. However, the efforts to quantify the IWC losses by counting the incoming ice particles that approach the sensor cone and rebound out based on high-speed video frames proved unsuccessful.

The ice particles produced in the Cox & Co. wind tunnel studies may have a higher density and less fragile structure than many vapor-grown ice crystals. The OAP-2DC imagery indicates that the majority of the artificial ice particles produced in the wind tunnel had compact shapes (Emery et al. 2004). Such particles may behave like solid balls, resulting in elastic bouncing on impact with the sensor surface (see Fig. 3a). Because of these specific features inherent in the wind tunnel environment, it was decided to perform high-speed video studies during flight in natural clouds, where it is known that the turbulence, particle trajectories, and particularly the mechanical properties of ice particles could be different. A series of dedicated tests was conducted using the National Research Council (NRC) Convair-580 in December 2004 using a total of 16 flight hours (Isaac et al. 2006). The particles striking an original 120° TWC sensor of the Nevzorov probe were imaged using a Phantom v5 high-speed camera installed inside the fuselage of the Convair-580 and viewing the Nevzorov TWC sensor mounted approximately 50 cm off the fuselage skin.

Figure 2 shows a sequence of video frames capturing the impact of the spatial dendrite with the Nevzorov TWC cone. Image analysis of numerous similar impact events indicated that such ice particles shattered into a large number of small ice fragments, a fraction of which were visibly swept away from the cone with the airflow. Arrows in Figs. 2b–d indicate the outflow of the small ice particle fragments, which resulted from the shattering of the dendrite shown in Fig. 2a before it entered the TWC cone.

The comparisons between the high-speed videos recorded in the wind tunnel and the natural cloudy

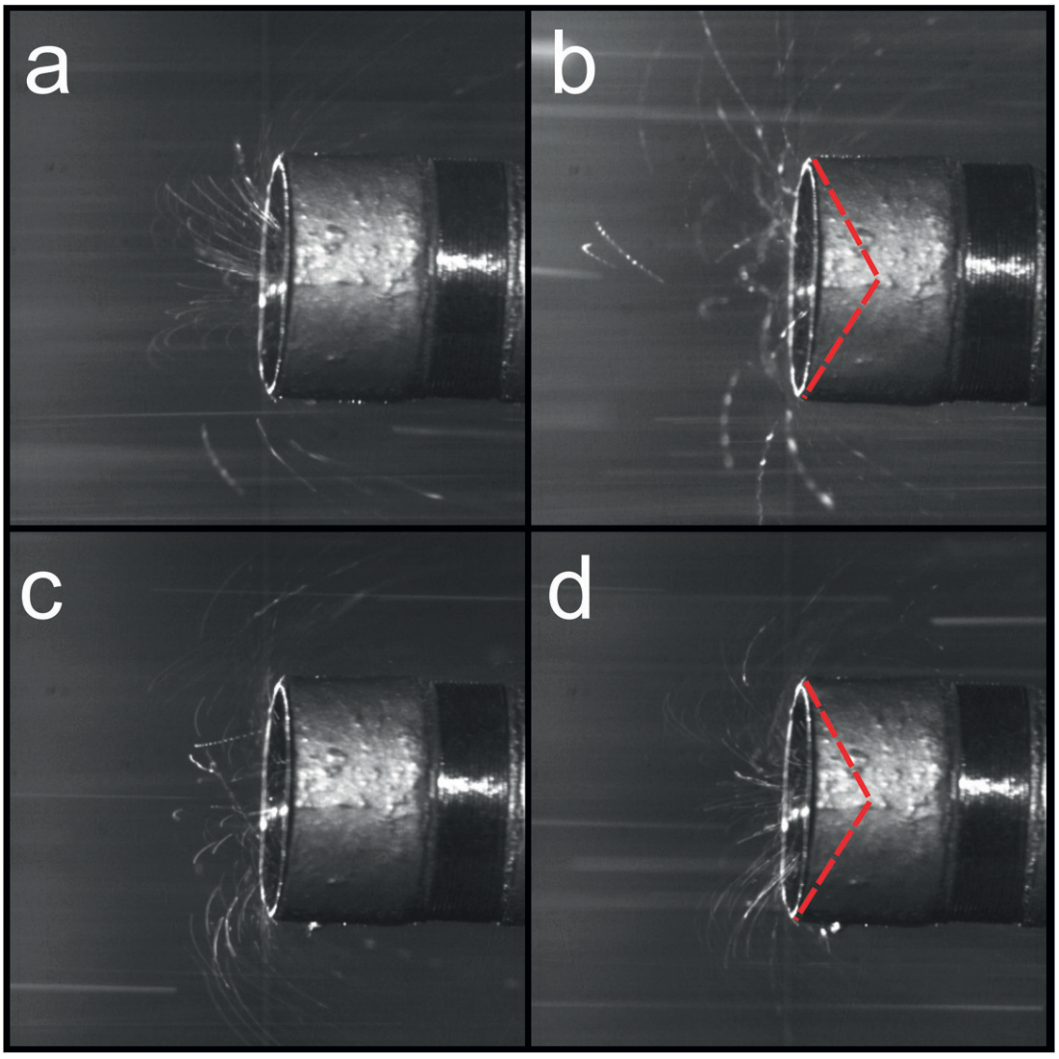

FIG. 1. Images of the Nevzorov TWC sensor cone taken with high-speed video camera in a flow of ice particles in the Cox & Co wind tunnel. Red dashed lines in (b) and (d) indicate the shape of the hollow cone of the hot-wire sensor. Airspeed is 80 m s^{-1}. Original video is available online at ftp://depot.cmc.ec.gc.ca/upload/hsvideo.

environment revealed differences in the behavior of artificial and natural ice particles after their impact with the TWC cone. On one hand, in a high-density case, the artificial ice particles may behave more like solid balls, with elastic bouncing on impact, whereas naturally grown ice particles with complex morphology and low densities, such as spatial dendrites, tend to shatter into a large number of small fragments. Some fraction of this shattered ice may be swept out of the cone by airflow (or may bounce from the surface), while the other fraction may be melted and evaporated and thus be measured by the probe. The conceptual diagram in Fig. 3 demonstrates the difference between the behaviors of artificial and complex natural ice particles of this type. It is reasonable to assume that natural ice particles with more compact geometry and higher mass densities may behave similarly to the artificial ice produced in tunnels, although no such data were available from the flight tests with the high-speed video.

Strapp et al. (2005) compared the response of hot-wire sensors of different geometry to shaved ice particles in the Cox & Co. icing wind tunnel, showing that a 16-mm-deep sensor displayed far fewer particles bouncing out of the capture volume than the 2-mm-deep Nevzorov shallow sensor. Furthermore, the 16-mm-deep sensor measured at least 2 times larger IWC than the standard Nevzorov shallow sensor. This work indicated that the efficiency of the capture of ice particles by hot wires could potentially be increased greatly by modifications to the sensor geometry.

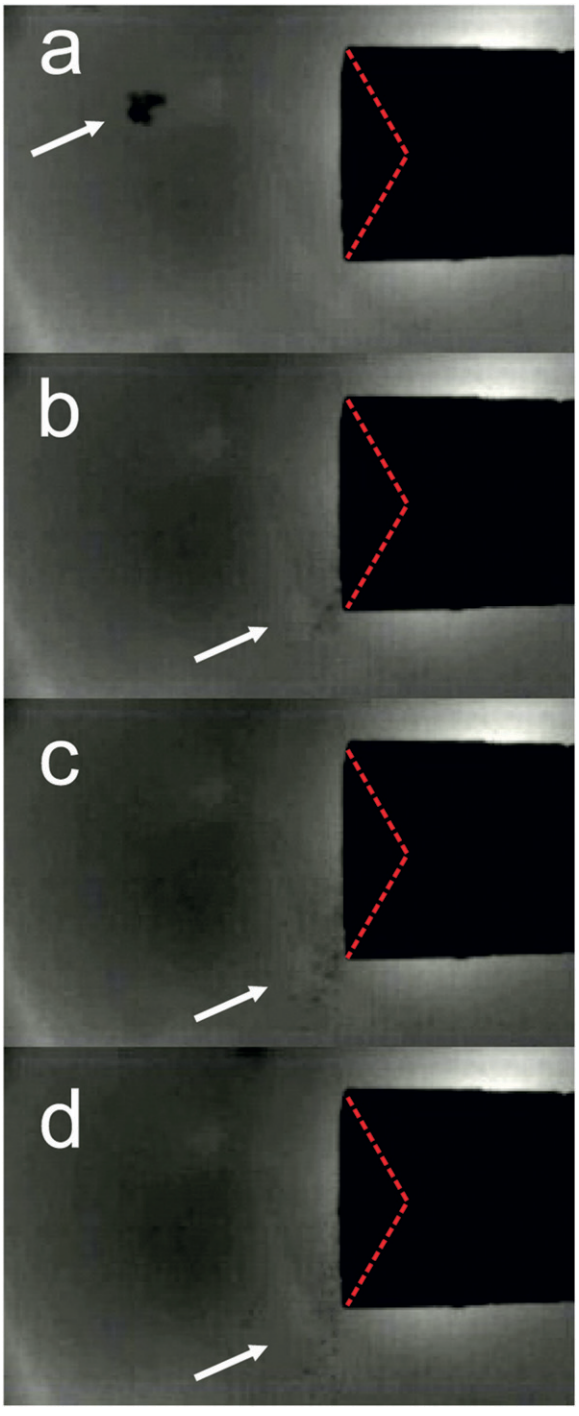

FIG. 2. Sequence of frames captured by the high-speed video camera showing the impact of a 1-mm spatial dendrite with the standard (120° cone) Nevzorov TWC hot-wire sensor. Arrow in (a) indicates the spatial dendrite before impact with the hot-wire cone, and arrows in (b)–(d) point to the outflow of the ice particle fragment powder that resulted from the shattering. Measurements were obtained during the NRC Convair-580 flight in nimbostratus on 18 Dec 2004. Red dashed lines indicate the shape of the hot-wire sensor cone. See Isaac et al. (2006) for details of the test. Original video is available online at ftp://depot.cmc.ec.gc.ca/upload/hsvideo.

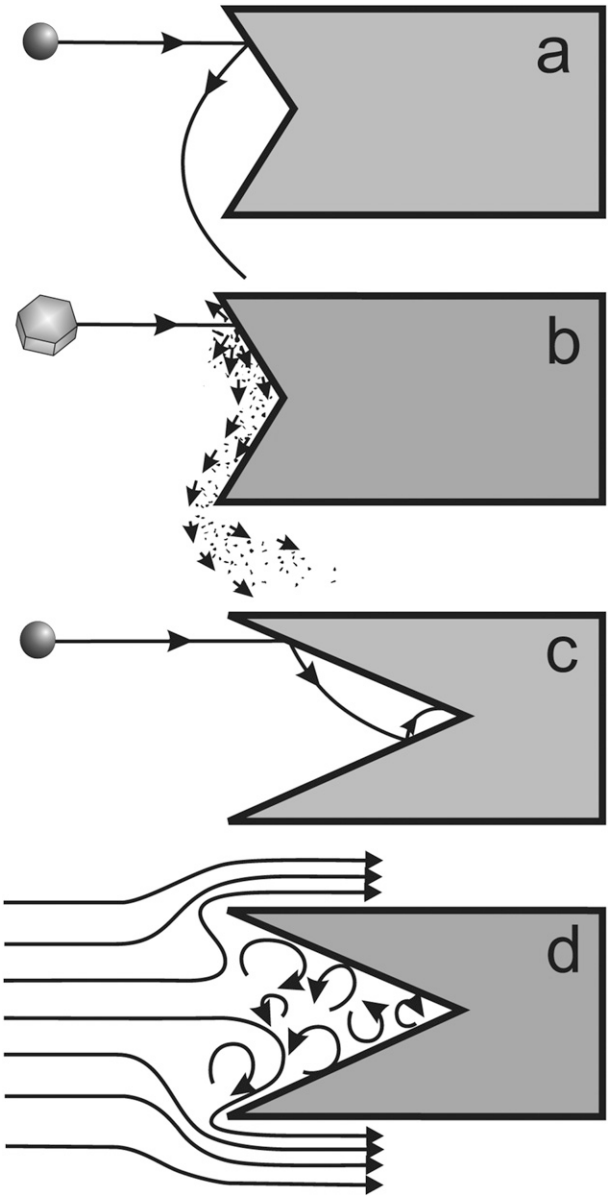

FIG. 3. Conceptual diagram of the (a) elastic and (b) inelastic bouncing of ice particles with shallow TWC sensor cone, (c) elastic bouncing of ice particles in the deep TWC sensor cone, and (d) vorticity inside the deep cone.

The fraction of the rebound particles is anticipated to depend on the geometrical characteristics of the sensor. The ice particles striking a shallow Nevzorov cone with its wide cone angle are expected to experience just one bounce before they potentially exit the sensor (Fig. 3a). However, ice particles entering a cone with a sharper interior angle may bounce several times within the cone's surface, thus reducing the probability of exiting the sensor before their complete evaporation (Fig. 3c). Using this concept in an attempt to reduce the ice

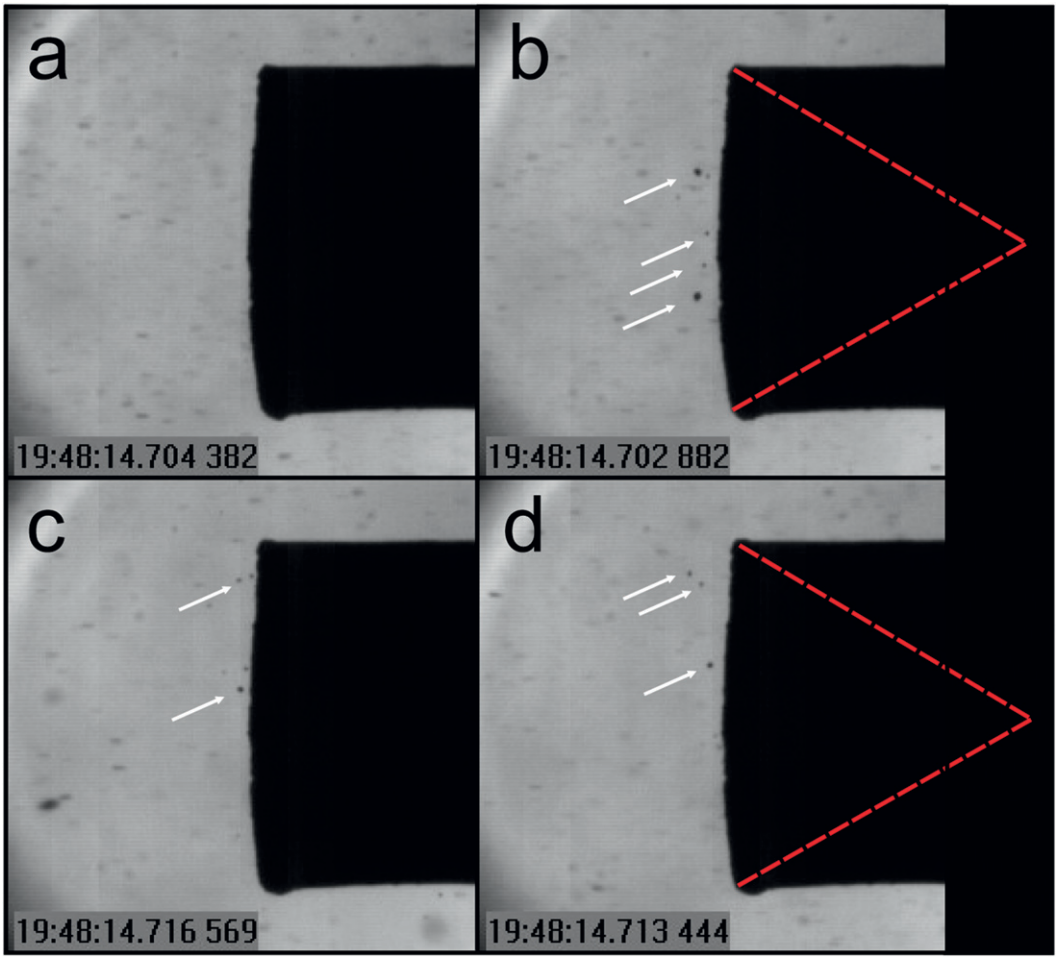

FIG. 4. Images of the modified (60° cone) Nevzorov TWC sensor taken with the high-speed camera in the flow of ice particles in the Cox & Co. wind tunnel. Arrows in (b) indicate the ice particles rebounding from the cone. Rebounding ice particles in (b)–(d) appear as quasi-circular images. Image frame in (a) does not contain rebounded particles. Red dashed lines in (b) and (d) indicate the shape of the hollow cone of the hot-wire sensor. Airspeed is 80 m s^{-1}. Original video is available online at ftp://depot.cmc.ec.gc.ca/upload/hsvideo.

bouncing efficiency, a special ''deep'' TWC sensor cone was constructed with a 60° angle. This also resulted in a deeper catch volume requiring particles to bounce farther forward into the airstream to exit the capture volume.

Figure 4 shows video frames of the modified deep TWC cone exposed to the flow of ice particles. The video in this sequence was shot with a different exposure rate that does not result in the particle streaks observed in Figs. 1a–d. The bounced particles in this video appear as quasi-spherical sharp images, whereas the ice particles in the undisturbed flow appear as elongated streaks because of their higher velocity. The rebounding ice particles are indicated by the arrows in Fig. 4b. Most video frames of the deep cone did not contain evidence of particles bouncing out of the capture cone and appear like that shown in Fig. 4a. This observation suggests that the new deep cone TWC sensor has a better efficiency for capturing and melting ice particles relative to the original shallow cone sensor.

The high-speed video gives a general idea whether ice particle bouncing exists or not. However, the quantification of the underestimation of IWC due to bouncing based on high-speed video analysis is hindered for many practical reasons, and it does not seem possible at the current stage. In particular, the shattering of fragile ice particles results in a large number of small ice fragments that cannot be accounted for in an estimate of mass loss, because they may not be visible on the image frames as a result of coarse pixel resolution and limited depth of field. Similarly, original particles smaller than the practical size limit of the camera also cannot be tracked.

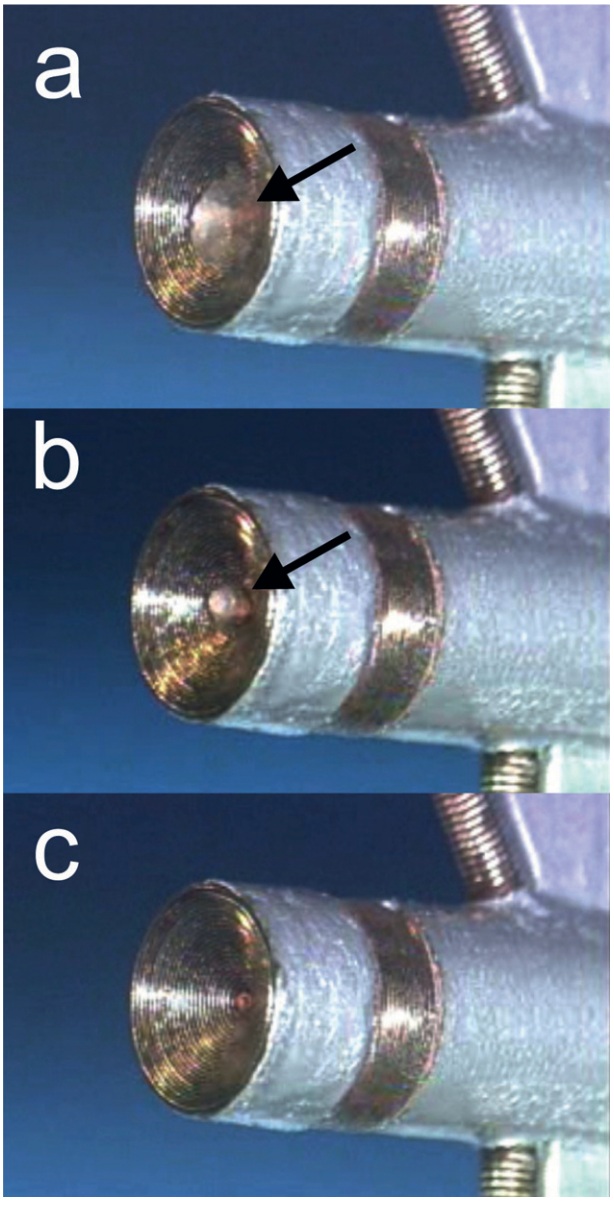

FIG. 5. (a),(b) Snapshots from the high-definition video demonstrating the pooling effect in the accumulation of nonevaporated water at the bottom of the TWC hot-wire cone. (c) Photo of the hot-wire cone without water.

Another source of underestimation of IWC results from incomplete evaporation of ice particles after melting inside the TWC hot-wire cone. If the mass concentration of ice particles is too high, then the power of the sensor is insufficient for evaporation of the condensed water captured by the cone. In this case melted water forms a pool at the bottom of the cone. Figure 5 shows images extracted from the high-definition video illustrating pools of the melted water inside the TWC cone. The effect of ''pooling'' was originally observed and described by Emery et al. (2004). The video sequences also show random movement of the pool of water due to aerodynamic instability in the cone, with the pool eventually being swept out of the cone and into the airflow. In the wind tunnel experiments, the duration of pooling from the moment of its formation to the expulsion from the cone was usually less than 1 s. Such pooling was observed only when the IWC measured by the shallow TWC cone exceeded approximately $0.7\,g\,m^{-3}$ (Emery et al. 2004). As will be shown below, the standard shallow Nevzorov IWC measurement is approximately 30% of the true values, implying that pooling would be observed only if the IWC exceeded approximately $2.1\,g\,m^{-3}$. Since the true IWC estimated from the in situ measurements discussed below does not exceed 0.6–$0.7\,g\,m^{-3}$, then the effect of pooling for the shallow cone is considered to be insignificant for the study. It is anticipated that for the deep cone, the threshold IWC for the pooling effect will be lower than $2.1\,g\,m^{-3}$ because of the configuration of the sensor. Unfortunately, the video camera set up in the Cox & Co. wind tunnel did not allow viewing the bottom of the cone, and therefore the threshold IWC for the pooling for the deep cone TWC sensor at the moment remains unknown. However, the linear dependence between IWC measured in situ by the deep and shallow TWC cones (section 3, Fig. 8a) suggests that the effect of pooling is insignificant for the deep cone for this study as well.

3. In situ comparisons of IWC techniques

To characterize the underestimate of IWC due to bouncing, the standard Nevzorov shallow (120° cone) and new prototype deep (60° cone) TWC sensors were mounted on the same sensor vane (Fig. 6a). This configuration allows for simultaneous measurements of IWC by both sensors. The Nevzorov probe along with the CVI component (Twohy et al. 1997) of the DMT CSI (Fig. 6b) and PMS OAP-2DC and OAP-2DP (Knollenberg 1981) were mounted on the NRC Convair-580. The measurements of IWC were obtained from glaciated clouds measured during the Canadian *CloudSat*/*Cloud–Aerosol Lidar and Infrared Pathfinder Satellite Observations* (*CALIPSO*) Validation Project (C3VP) in southern Ontario, Canada (Barker et al. 2008).

The pixel resolutions of the OAP-2DC and OAP-2DP were set to 25 and 200 μm, respectively. The OAP-2DC was equipped with antishattering tips to mitigate the effect of ice particle shattering on the measurements (Korolev et al. 2011, 2013). The remaining artifact images related to shattering were filtered out with the help of an interarrival time algorithm (e.g., Field et al. 2006).

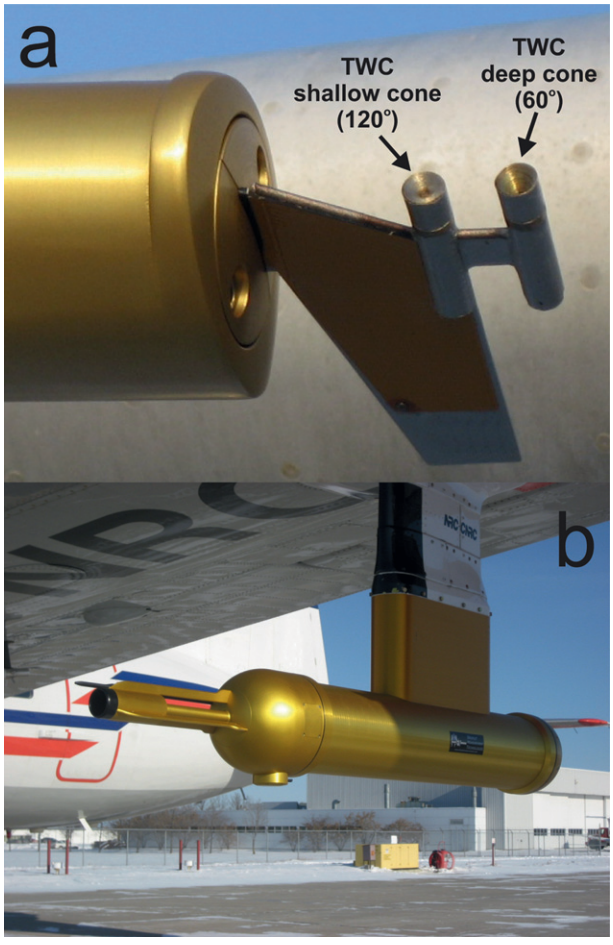

FIG. 6. Modified Nevzorov sensor head; (a) both shallow and deep sensors mounted on the same vane and (b) DMT CVI probe installed on the NRC Convair-580.

The diameter of the CVI inlet tube used in this study was 4.4 mm. The inlet tube was mounted at the back of the shroud (Fig. 6b), which was installed for stabilizing the airflow during the aircraft maneuvers (pitching, changing angle of attack and yaw, etc.). The particle cut size was calculated by the supplier to be about 7 μm for a unit density sphere and 100 m s^{-1} at 850 mb, although there is some wind tunnel evidence that LWC underestimation may be significant in liquid cloud with mean volume diameters (MVDs) up to approximately 30 μm, with around 40% underestimation at an MVD of 20 μm (Twohy et al. 2003). The latter performance would appear to be more consistent with airborne liquid-cloud LWC comparisons of the CSI to hot-wire instruments with trusted accuracy performed by Environment Canada, although no comprehensive airborne comparisons have been performed to date. Nevertheless, since the efficiency of the CSI can be assumed to be roughly the same for small water droplets and ice particles of the

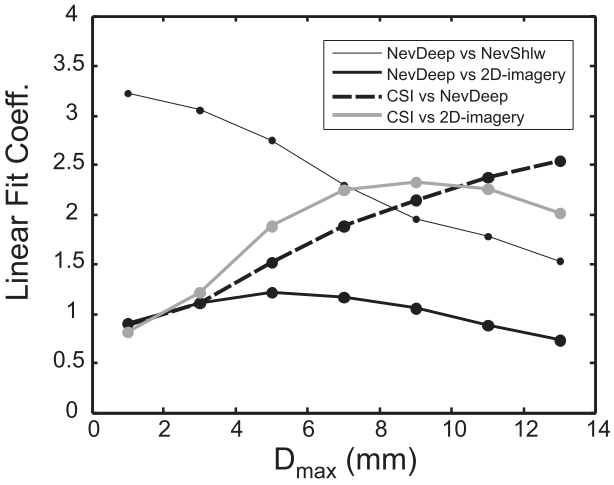

FIG. 7. Linear fit coefficient vs D_{max} for pairs of different IWC instruments indicated in the legend. Each data point on the diagram was calculated for 2-mm interval of D_{max} centered, as indicated by circles.

same size because of the quasi-spherical shape and similar density, and since the particle spectra for the most cases reveal that the mass is concentrated at sizes much larger than 30 μm, the issue of the CSI cut size can be concluded to be insignificant for the ice clouds considered in this study. The calculation of the mass of ice particles from their 2D imagery was performed based on the size-to-mass parameterization $M = aD^b$ (Mason 1957). The coefficients $a = 7.38 \times 10^{-11}$ and $b = 1.9$ were taken from Brown and Francis (1995), as originally determined by Locatelli and Hobbs (1974) for "aggregates of unrimed bullets, columns, and side plates." IWC was computed by integrating the mass of ice particles over the size distribution measured by the OAP-2DC and OAP-2DP. To improve the statistical significance of the particle size distributions, the OAP data were averaged over 4-s time intervals. The measurements of the Nevzorov probe and CVI were averaged over the same time intervals in order to synchronize all measurements and to enable the direct intercomparisons of all probes. Heymsfield et al. (2010) have empirically derived updated a and b coefficients for different cloud regimes that exhibit effective density discrepancies from Brown and Francis (1995) of up to a factor of 2, generally increasing with particle size. Therefore, some caution must be placed on the interpretation of 2D-derived IWC values compared to the other instruments, which have measurements much closer to first principles.

The comparisons reveal that the four IWC measurement techniques are all linearly related. However, the linear fit slope coefficient is a function of the size of ice particles. Figure 7 shows the dependence of the linear fit coefficient on the maximum size D_{max} of ice particles in

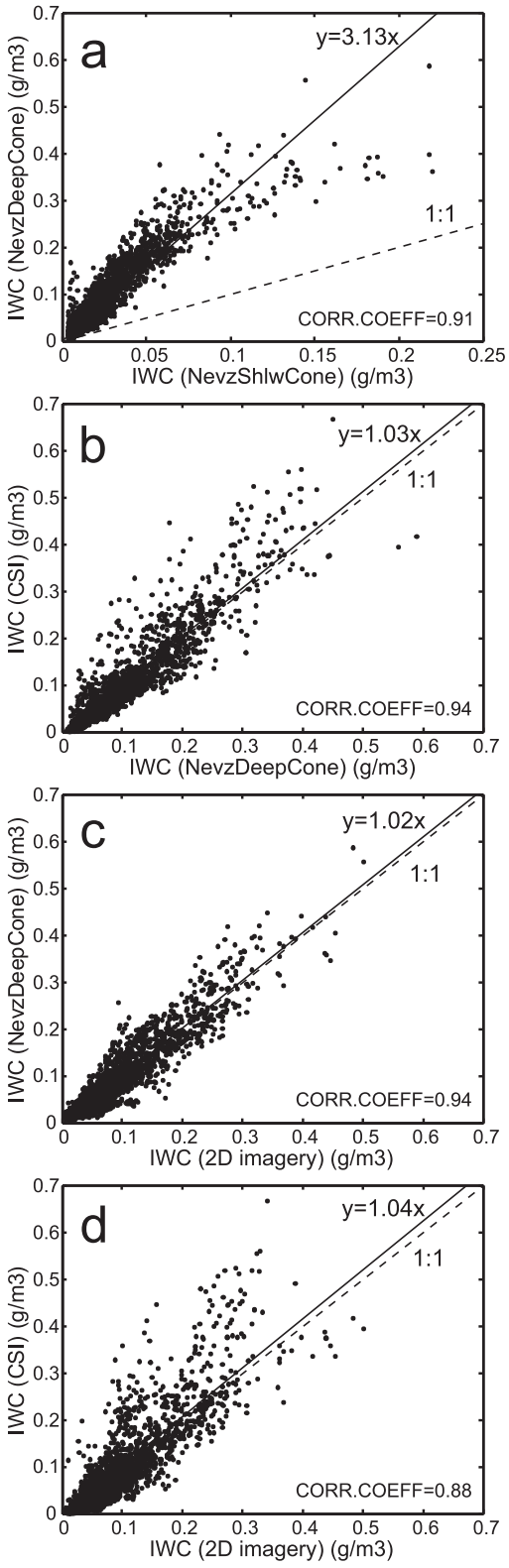

FIG. 8. Scatter diagrams of IWC measured by the Nevzorov deep and shallow TWC sensors, DMT CVI, and OAP-2DC and OAP-2DP in ice clouds with $D_{max} < 4$ mm. Averaging time $\Delta t = 4$ s.

the measured size distributions. The size D_{max} was defined from the 2D measurements as a maximum particle size in the ensemble of ice particles sampled during the 4-s averaging interval. The results show that the ratio of IWC measured by different instruments changes with the maximum particle size. Interestingly, the IWC measured by the Nevzorov deep cone agrees reasonably well with that deduced from the OAP size distributions for the whole size range. Figure 7 indicates that for ice particle clouds with $D_{max} < 4$ mm, the Nevzorov deep cone gives very similar IWC values to the CVI. For clouds with large ice particles ($D_{max} > 10$ mm), the IWC measured by the CVI is more than 2 times greater than that measured by the Nevzorov deep cone. At all particle sizes, the Nevzorov shallow cone measures a factor of 1.5 or more lower than the other probes, and is clearly the probe with the lowest readings.

Figure 7 identifies a markedly different response behavior between the probes for ice distributions with $D_{max} > 4$ mm versus those with $D_{max} < 4$ mm. Figure 8 shows scatter diagrams of IWC measured by different pairs of instruments for the ice clouds with particle $D_{max} < 4$ mm. As seen in Fig. 8a, the IWC measured by the Nevzorov deep cone sensor is approximately 3 times larger than that measured by the shallow cone. The rest of the probes—the Nevzorov deep cone, CVI, and size-to-mass conversion from 2D imagery—agree relatively well with one another for ice clouds with particle $D_{max} <$ 4 mm. Figure 9 shows the scatter diagrams of IWC measured by the same pairs of probes but with particle $D_{max} > 4$ mm. For these clouds, the correlation between the IWC measurements is degraded and the linear fit coefficients change such that the ratio of the Nevzorov deep cone sensor is now approximately 2 times larger than the shallow cone sensor.

It is worth mentioning that most ice clouds with large ice particles ($D_{max} > 4$ mm) were associated with temperatures $-15° < T < -10°$C (Fig. 10a). This temperature range corresponds to the dendritic ice growth regime. Dendrites typically form large fragile low-density aggregates that may be hypothesized to cause larger measurement problems because of fragmentation and shattering. As seen from the diagrams in Figs. 9, these particles result in the largest uncertainties in IWC measurements and therefore IWC measurements under these conditions may require special attention and uncertainty consideration.

The results of this study do not allow for an unambiguous conclusion as to which instrument provides the most accurate result in this region of maximum discrepancy. Perhaps large dendrite conditions are conducive to underestimation of IWC by the Nevzorov deep cone sensor, caused by vorticity in the cone

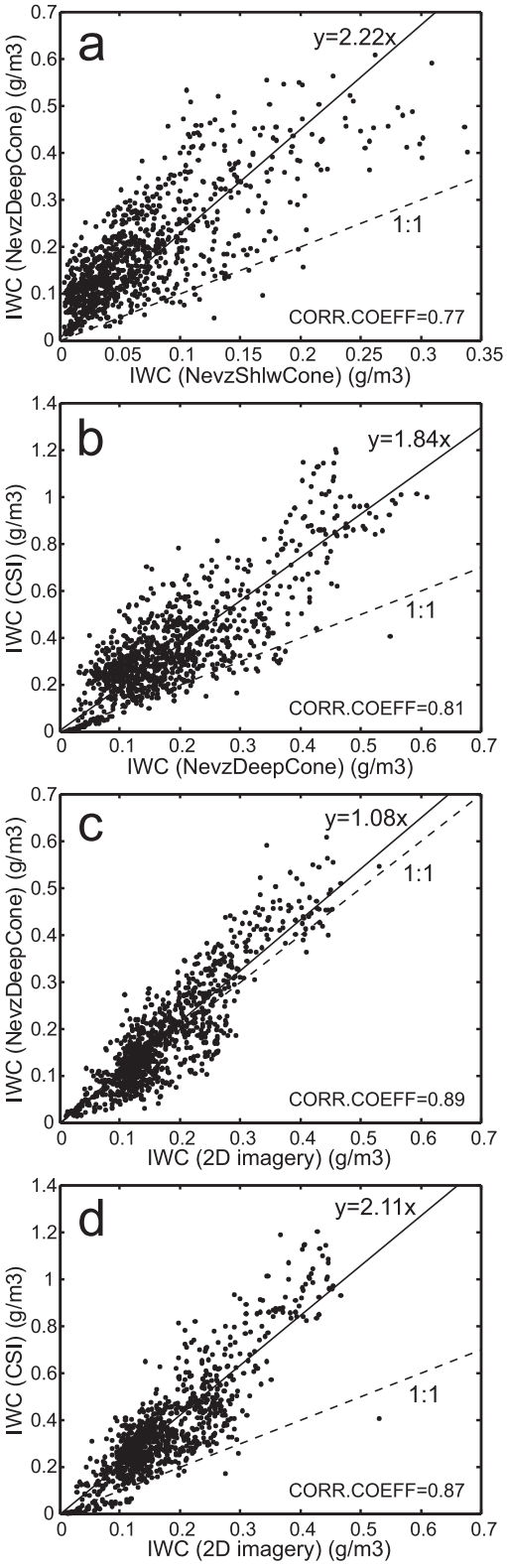

FIG. 9. As in Fig. 8, but for $D_{max} > 4$ mm.

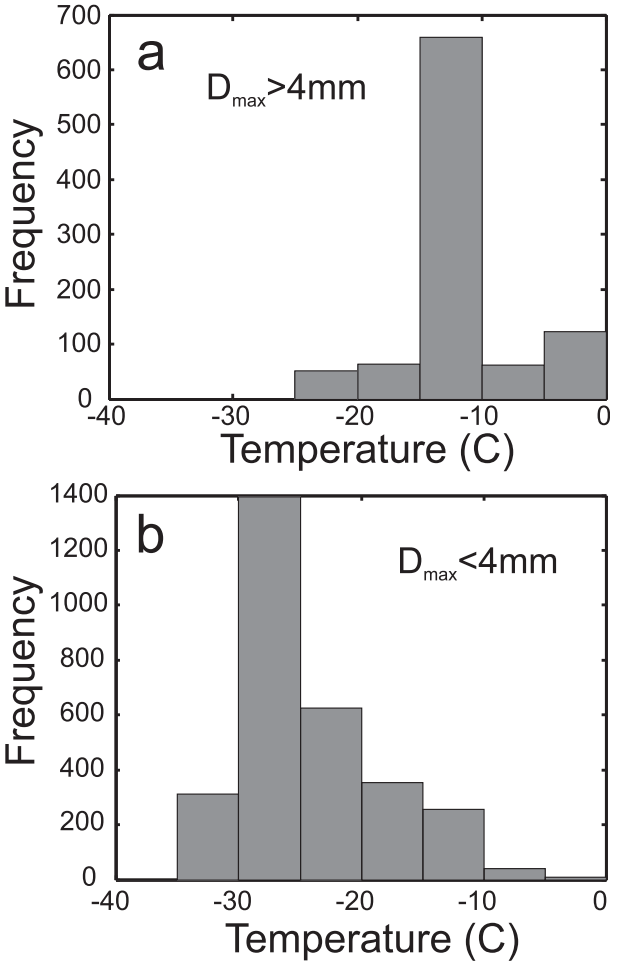

FIG. 10. Frequency distribution of temperatures corresponding to data presented (a) in Fig. 9 (ice particle $D_{max} > 4$ mm) and (b) in Fig. 8 (ice particle $D_{max} < 4$ mm).

sweeping away miniscule shattered particles, as observed in Fig. 3d. On the other hand, an overestimation of IWC measured by the CVI for $D_{max} > 4$ mm may be caused by the bouncing of shattered dendrites colliding with the rounded shroud, with a subsequent focusing of the debris on the CVI inlet tube. Some support for this assumption is provided by the well-established effect of bouncing of ice particles from the leading edge of the forward scattering spectrometer probe (FSSP) inlet tube (Field et al. 2003), similar in dimensions and layout to the CVI sample tube, with its subsequent contamination of the FSSP sample area inside the tube (Korolev et al. 2013).

4. Conclusions

The data from this study support the following conclusions. First, IWC measurements taken by the new

prototype Nevzorov deep cone and DMT CVI, and IWC calculated from OAP particle size spectra agree within 50% for ice clouds with ice particle $D_{max} < 4$ mm. This agreement suggests that all three techniques may provide reasonably consistent IWC measurements for ice particles with $D_{max} < 4$ mm. When larger ice particles are present, the CVI measures increasingly larger IWC values than the Nevzorov deep cone (factor of 2–2.5 for $D_{max} > 8$ mm). Although caution must be exercised in the interpretation of comparisons to IWC derived from optical array probe images, it is interestingly to note that IWC measured by the Nevzorov deep cone and that estimated by applying mass–diameter relationships of Brown and Francis (1995) to OAP imagery are approximately equal throughout the entire range of ice particle sizes.

Next, for ice particle spectra with $D_{max} < 4$ mm, the IWC measured by the standard Nevzorov shallow cone is approximately 3 ± 0.2 times lower than that measured by the Nevzorov deep cone and CVI. Assuming that the close agreement between the CVI and the deep cone indicates that both are measuring approximately correctly, this allows for approximate corrections of IWC datasets collected with the Nevzorov shallow cone TWC sensor during previous flight campaigns, in cases where large particles ($D_{max} > 4$ mm) are not present. The correction must take into account any liquid fraction in the cloud, which will be measured at a much higher efficiency.

Last, the results do not allow for an unambiguous conclusion about the accuracy of IWC measurement devices when large dendrites and aggregated ice particles are present ($D_{max} > 4$ mm), and when the CVI measurements diverged from the deep cone and the OAP estimates described earlier. More studies are required to resolve this problem.

Acknowledgments. Many thanks are given to Vincent Reich from NASA Glenn for providing the high-speed video equipment during the Cox & Co. wind tunnel tests and the in situ sampling on the NRC Convair-580. The aircraft data were obtained using the NRC Convair-580 and the scientific and technical efforts of many NRC and MSC staff. A special thanks is given to the Cox & Co. personnel and, in particular, to Adam Lawrence for a high level of cooperation and support in operating the Cox & Co. wind tunnel facility. The Canadian Space Agency (CSA) provided funding for the C3VP aircraft projects. The Federal Aviation Administration as well as NASA Glenn provided support for the in situ measurements in 2004. Transport Canada has provided support for all of this work. The authors also express their gratitude to three anonymous reviewers for their thoughtful comments and valuable suggestions.

REFERENCES

Baker, B., and R. P. Lawson, 2006: Improvement in determination of ice water content from two-dimensional particle imagery. Part I: Image-to-mass relationships. *J. Appl. Meteor. Climatol.,* **45,** 1282–1290.

Barker, H. W., A. V. Korolev, D. R. Hudak, J. W. Strapp, K. B. Strawbridge, and M. Wolde, 2008: A comparison between CloudSat and aircraft data for a multilayer, mixed phase cloud system during the Canadian CloudSat-CALIPSO Validation Project. *J. Geophys. Res.,* **113,** D00A16, doi:10.1029/2008JD009971.

Brown, P. R. A., 1993: Measurements of the ice water content in cirrus using an evaporative technique. *J. Atmos. Oceanic Technol.,* **10,** 579–590.

——, and P. N. Francis, 1995: Improved measurements of the ice water content in cirrus using a total-water probe. *J. Atmos. Oceanic Technol.,* **12,** 410–414.

Davis, S. M., A. G. Hallar, L. M. Avallone, and W. Engblom, 2007: Measurement of total water with a tunable diode laser hygrometer: Inlet analysis, calibration procedure, and ice water content determination. *J. Atmos. Oceanic Technol.,* **24,** 463–475.

Davison, C. R., J. D. MacLeod, and J. W. Strapp, 2009: Naturally aspirating isokinetic total water content probe: Evaporator design and testing. Preprints, *First AIAA Atmospheric and Space Environments Conf.,* San Antonio, TX, AIAA, AIAA 2009-3861, doi:10.2514/6.2009-3861.

Emery, E. F., D. R. Miller, S. R. Plaskon, J. W. Strapp, and L. Lilie, 2004: Ice particle impact on cloud water content instrumentation. Preprints, *42nd AIAA Aerospace Sciences Meeting and Exhibit,* Reno, NV, AIAA, AIAA 2004-0731.

Field, P. R., R. Wood, P. R. A. Brown, P. H. Kaye, E. Hirst, R. Greenaway, and J. A. Smith, 2003: Ice particle interarrival times measured with a fast FSSP. *J. Atmos. Oceanic Technol.,* **20,** 249–261.

——, A. J. Heymsfield, and A. Bansemer, 2006: Shattering and particle interarrival times measured by optical array probes in ice clouds. *J. Atmos. Oceanic Technol.,* **23,** 1357–1370.

Heymsfield, A. J., C. Schmitt, A. Bansemer, and C. H. Twohy, 2010: Improved representation of ice particle masses based on observations in natural clouds. *J. Atmos. Sci.,* **67,** 3303–3318.

Isaac, G. A., A. V. Korolev, J. W. Strapp, S. G. Cober, F. S. Boudala, D. Marcotte, and V. L. Reich, 2006: Assessing the collection efficiency of natural cloud particles impacting the Nevzorov total water content probe. Preprints, *44th Aerospace Sciences Meeting and Exhibit,* Reno, NV, AIAA, AIAA 2006-1221, doi:10.2514/6.2006-1221.

King, W. D., and D. E. Turvey, 1986: A thermal device for aircraft measurement of the solid water content of clouds. *J. Atmos. Oceanic Technol.,* **3,** 356–362.

Knollenberg, R. G., 1981: Techniques for probing cloud microstructure. *Clouds: Their Formation, Optical Properties, and Effects,* P. V. Hobbs and A. Deepak, Eds., Academic Press, 15–91.

Korolev, A. V., J. W. Strapp, G. A. Isaac, and A. N. Nevzorov, 1998: The Nevzorov airborne hot-wire LWC–TWC probe: Principle of operation and performance characteristics. *J. Atmos. Oceanic Technol.,* **15,** 1495–1510.

——, E. F. Emery, J. W. Strapp, S. G. Cober, G. A. Isaac, M. Wasey, and D. Marcotte, 2011: Small ice particles in tropospheric clouds: Fact or artifact? Airborne Icing Instrumentation Evaluation Experiment. *Bull. Amer. Meteor. Soc.,* **92,** 967–973.

——, ——, and K. Creelman, 2013: Modification and tests of particle probe tips to mitigate effects of ice shattering. *J. Atmos. Oceanic Technol.,* **30,** 690–708.

Kyle, T. G., 1975: The measurement of water content by an evaporator. *J. Appl. Meteor.,* **14,** 327–332.

Locatelli, J. D., and P. V. Hobbs, 1974: Fall speeds and masses of solid precipitation particles. *J. Geophys. Res.,* **79** (C15), 2185–2179.

Mason, B. J., 1957: *The Physics of Clouds*. Oxford University Press, 671 pp.

Nevzorov, A. N., 1980: Aircraft cloud water content meter. *Communications à la VIIIème Conférence Internationale sur la Physique des Nuages,* Vol. II, AIMPA, 701–703.

——, 1983: Aircraft cloud water content meter (in Russian). *Trans. Central Aerological Obs.,* **147,** 19–26.

Nicholls, S., J. Leighton, and R. Barker, 1990: A new fast response instrument for measuring total water content from aircraft. *J. Atmos. Oceanic Technol.,* **7,** 706–718.

Ruskin, R. E., 1967: Measurements of water-ice budget changes at −5C in AgI-seeded tropical cumulus. *J. Appl. Meteor.,* **6,** 72–81.

——, 1976: Liquid water content devices. Atmospheric Technology, Vol. 8 (spring), NCAR, 38–42.

Strapp, J. W., L. E. Lilie, E. E. Emery, and D. Miller, 2005: Preliminary comparison of ice water content as measured by hot wire instruments of varying configuration. Preprints, *43rd AIAA Aerospace Sciences Meeting and Exhibit,* Reno, NV, AIAA, AIAA 2005–0860, doi:10.2514/6.2005-860.

——, J. MacLeod, and L. E. Lilie, 2008: Calibration of ice water content in a wind tunnel/engine test cell facility. *Proc. 15th Int. Conf. on Clouds and Precipitation,* Cancun, Mexico, ICCP, P13.1. [Available online at http://cabernet.atmosfcu.unam.mx/ICCP-2008/abstracts/Program_on_line/Poster_13/StrappEtAl-extended.pdf.]

Twohy, C. H., A. J. Schanot, and W. A. Cooper, 1997: Measurement of condensed water content in liquid and ice clouds using an airborne counterflow virtual impactor. *J. Atmos. Oceanic Technol.,* **14,** 197–202.

——, J. W. Strapp, and M. Wendisch, 2003: Performance of a counterflow virtual impactor in the NASA Icing Research Tunnel. *J. Atmos. Oceanic Technol.,* **20,** 781–790.

Weinstock, E. M., and Coauthors, 2006: Measurements of the total water content of cirrus clouds. Part I: Instrument details and calibration. *J. Atmos. Oceanic Technol.,* **23,** 1397–1409.